Chapter 9 – Discharge Scenarios

Our objective in developing the discharge scenarios is to judge whether there are plausible and reasonable paths from vacuum fields to the desired NCSX target equilibrium. Our primary focus is the CDR reference configuration based on the PVR reference configuration li383_328 with minor shape modification resulting from free boundary optimization with the M45 healed coil set, M45h. Much of the physics addressed here in pursuit of this goal is the evolution of the plasma poloidal flux. In addition to the vacuum transform, NCSX plasmas have significant toroidal current which is largely bootstrap driven. Neutral beams heat the plasma and there is the associated neutral beam current drive. Finally, there is the directly controllable component, Ohmic current driven via a central solenoid. All contribute to the iota profile, some in competing ways. There is not a developed simulation tool for following flux evolution in 3-D; however, as the device is quasi-axisymmetric we expect the usual tokamak tools to provide an accurate guide. The discharge evolution is followed using TRANSP, a 1 /2-D transport code with a high level of sophistication and maturity. The other major code used here is the STELLOPT optimization suite, based on VMEC. For the most part VMEC is used in its free-boundary mode with internal current and pressure profiles generated via TRANSP simulations, and searches for coil currents that retain attractive physics properties with these profiles.

There are four components to this task. First mapping the reference stellarator configuration into a 2-D "equivalent tokamak", called <NCSX>. Simulations are then developed to evolve the current profile from discharge initiation to the desired high beta state. Third, the profiles are mapped back into the 3-D configuration while solving the free-boundary equilibria to obtain the coil currents. A series of optimizations is performed for each time slice. Finally, the quality of the flux surfaces is verified.

9.1 Creating <NCSX>

As stated above the reference configuration is the starting point for the analysis. The reference equilibrium is specified by its 3-D shape and its internal profiles (pressure and current). The first step is to remove the plasma pressure and internal current to obtain the vacuum iota. The next step is to make an axisymmetric equilibrium, retaining only the n=0 components of the reference. Here (and only here) VMEC is run in the mode where the vacuum iota is preserved, rather than a current profile. As we have only axisymmetric terms this VMEC run then calculates the current profile needed to obtain this iota. This current profile is all that is needed from this calculation. This current, designated I_{EXT} is 321 kA for the R·B value of 2.05 T-m of the reference case. This transformation does not preserve aspect ratio nor plasma volume. We repeat, with a second axisymmetric calculation, keeping the n=0, m=0 term, but adjusting the n=0, m≠0 components by a single scale factor to restore the original aspect ratio, 4.37. In both cases we are keeping the value of toroidal flux at the boundary fixed at the reference equilibrium value. Since we retain the vacuum iota, the major radius, the plasma volume and the edge toroidal flux, the new <NCSX> equilibrium has a new R·B, or B since R of <NCSX> = <R> of the stellarator equilibrium. With this prescription <NCSX> has R·B=1.84 T-m and R=1.42 m. This will produce profiles with I_p, and $\Phi(\rho=1)$ values which correctly map back into the stellarator with R·B =2.05. Since we are not able to retain the wobble of the magnetic axis, there is not a unique

mapping to two dimensions. If we think of iota in terms of poloidal and toroidal currents, $\iota \propto R^2 I_{TOR} / (a^2 I_{POL}) = R I_{TOR} / (a^2 B) = R I_{TOR} / \Phi_{edge}$. Matching ι at a specified Φ_{edge} with I_{TOR} constrained, uniquely, allows for only B_ϕ as the freedom to preserve the boundary iota value. We maintain the vacuum iota constant (as a function of ρ) in time. This implies running a discharge at essentially constant shape. This is not the only choice one could make, but it seems the simplest and has yielded good results. The <NCSX> "vacuum" equilibrium flux surfaces and current profile are shown in Figure 9-1.

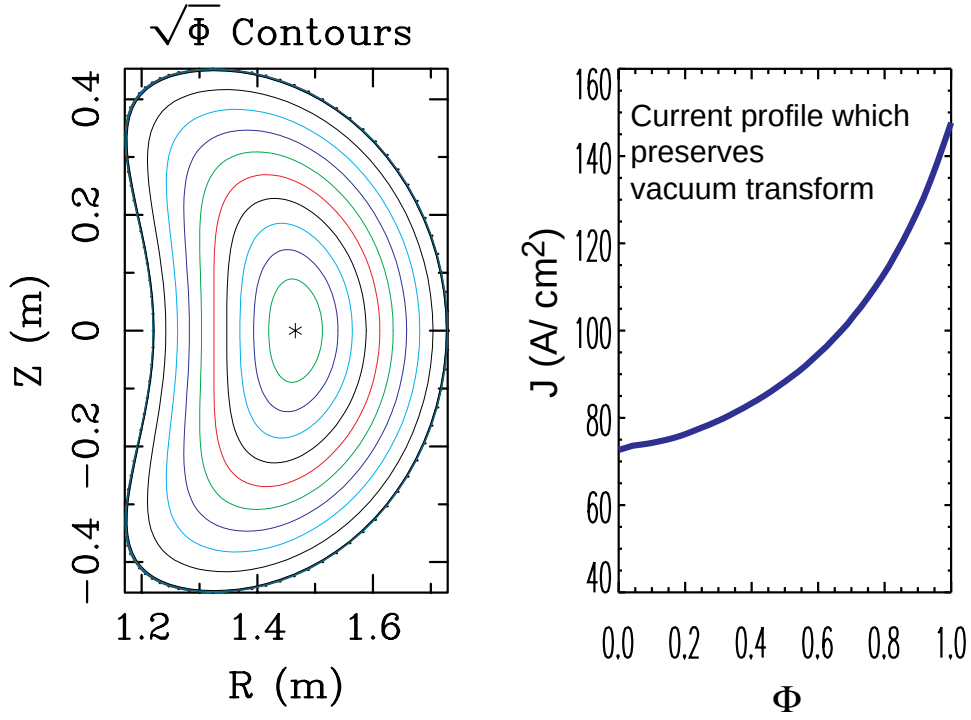

Figure 9-1. (a). Flux surfaces for the axisymmetric components of the shape of the target equilibrium, li383_328, at β=0, I_P=0 and (b). The toroidal current density producing the vacuum transform in the absence of 3D shaping

9.2 Discharge Evolution Modeling

The modeling of the current profile is done using TRANSP. The evolution of the density and Z_{eff} are specified in a way consistent with observations in small stellarators and tokamaks. The plasma current has two distinct components: The 321 kA equivalent of the vacuum iota is simulated as an externally specified, unchanging lower hybrid driven current (LHCD) profile. TRANSP allows this driven current profile input to be completely specified, without any other modeling of the standard LHCD process. Other physics assumptions of importance are using the NCLASS models for bootstrap current and neoclassical resistivity. The NCLASS calculations, which do more accurate (numerical) integrals of the distribution function, result in about a 13% decrease in bootstrap current, when compared to the usual analytic approximations. While neoclassical resistivity is similar outside the half-radius, near the axis the NCLASS calculation results in a 40% increase. Before proceeding we need to describe this use of TRANSP;

TRANSP is an analysis code, not really a simulator. The simulations are done iteratively: do a run, look at results, change something and do it again -- very much like running an experiment. This will be obvious in the plasma current. In order to obtain a current profile that is approximately constant in time (at the end of the pulse), it is quite important to minimize the Ohmic current during startup. When the plasma is cold, the current diffuses rapidly to the core. Once the plasma heats it will take a very long time to dissipate the Ohmic flux. The plasma current waveform, $I_P(t)$, represents a number of iterations where the old waveform is replaced with a new one, all intended to balance the OH current profile with neutral beam current drive (NBCD). The neutral beam injection is already a balance of co & counter beams, however this does not provide precise local cancellation across the plasma. During this iterative procedure an internal feedback loop in TRANSP is used to adjust the confinement time, to match a chosen global confinement scaling. Both χ_e and χ_I are adjusted to do this, by adjusting an anomalous diffusivity that is summed with analytic calculations of the neoclassical and helical ripple transport, as discussed in Chapter 7. The radial profile of the anomalous diffusivity is assumed to be flat as observed in many stellarator experiments. The global scaling we have adopted is the minimum of neo-Alcator and ITER97 L-mode scaling. Thus confinement is neo-Alcator at the beginning of the discharge and switches to ITER97L when the loss power becomes sufficiently large. Also, a switch is set in TRANSP to prevent the LHCD from experiencing the toroidal electric field, incorrectly developing Ohmic power.

The balance of the neutral beam powers is adjusted so that the larger counter-injection losses are compensated by a lower co-injected power. This is done so the effect of NBCD on central iota is not too severe, while overall the NBCD is not too negative. Co-injection orbit losses are about 18% and counter-injection losses are about 30%, similar to the calculations in Chapter 6. While the NCSX program will include an upgrade of the neutral beams to long pulse, initially they will be limited to a pulse length of 0.3 s. It is desirable to develop a scenario consistent with initial operation - despite the longer skin time of the plasma (~ 1.0 sec). The electron density profile is somewhat flattish as is common in small stellarators. The neutral beam pulses are modulated to control the heating power and produce the desired β_T.

As the design goal is a quasi-axisymmetric device, it is very useful to examine <NCSX> in some detail. We begin in Fig. 9-2 with the programmed quantities, plasma current, injected beam power and electron density, along with the loop voltage which is initially derived, then set to zero when the non-Ohmic current sources are sufficient. Recall that the plasma current sits on a pedestal of 321 kA representing the external transform. The density profile is consistent with observations in tokamaks and stellarators operating at this field value. As a guess, Z_{eff} is fixed at 2 in the center and the edge is set to rise modestly with time.

These simulations use the first 25 ms to get started, so the physical time is t-0.02. At 20 ms the conditions are a density of 1.1×10^{19} m^{-3}, and edge temperature of 10 eV and a central temperature of 50 eV for both ions and electrons. The q profile is that of the NCSX vacuum field. It is difficult to remove the first 25 ms and the reader should always ignore this part of the evolution. This time offset will persist through the chapter. When we speak of conditions at 303 ms, in a physical sense the time is 278 ms.

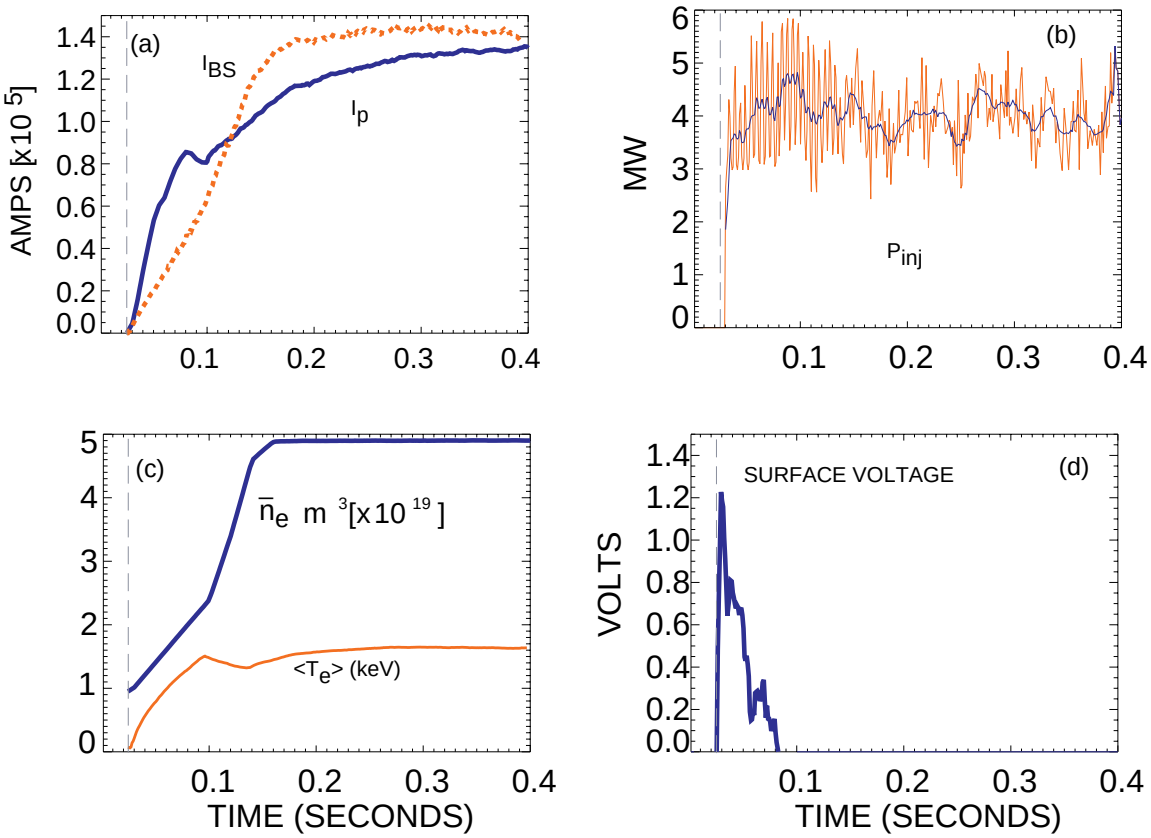

Figure 9-2. (a) Plasma current and bootstrap current, (b) Injected power and smoothed value, (c) line-averaged density and volume-averaged electron temperature, and (d) surface voltage. The dashed vertical line is the discharge initiation at 20 ms.

At the end of the discharge the plasma current is well matched to the bootstrap current. The loop voltage is programmed to zero after the initial current ramp. The neutral beam power is adjusted for the desired β by modulating the source current. The beam voltage here is 50 keV. The plasma density is programmed to rise with plasma current.
The confinement is time shown in Fig. 9-3 along with the scaling used.

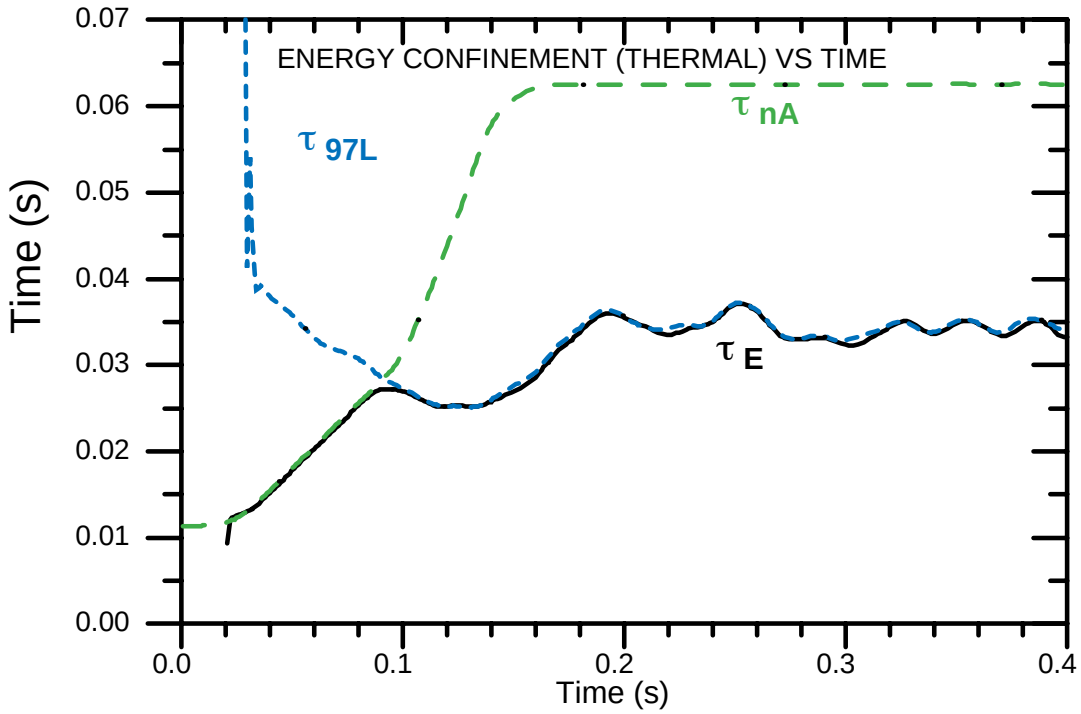

Figure 9-3. Energy confinement time, neo-Alcator scaling and ITER97L scaling.

In Fig. 9-4 we show selected physical parameters of the <NCSX> plasma. The collisionality is controlled by the confinement assumption through the anomalous diffusivities. Iota is a result of matching the total current to the bootstrap current. The total of 140 kA is less than the 175 kA of the reference plasma. There are a number of components to this difference: 30% of the plasma pressure is in fast ions, and these do not contribute to the bootstrap current. Then the pressure profile differs from the reference case because in our simulation the profile is controlled by the confinement assumptions. Finally, our assumptions result in different contributions from the density and temperature gradients. β_N/l_I is about 10, well above what would be stable to the external kink in a tokamak. The β is a result of the neutral beam programming. Note that the toroidal beta of 4% will correspond to an average β of 4.5% in the stellarator because of the different magnetic field normalization, volume-averaged B vs. toroidal field at the axis. The poloidal beta – 1.5 is not unusual for good performance in tokamaks. The normalization of these quantities is to the total equivalent current, $I_{EXT}+I_P$.

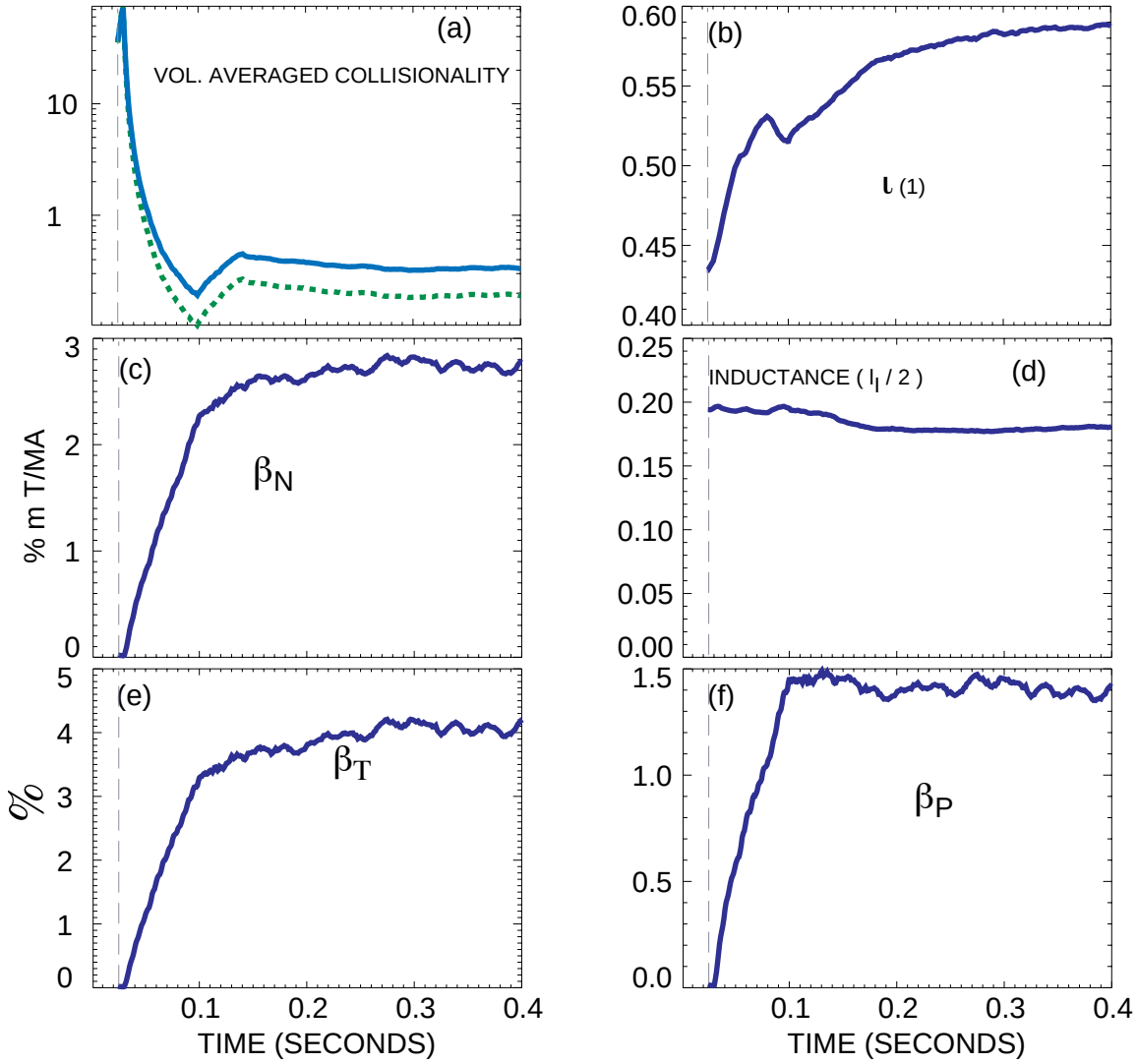

Figure 9-4. (a) Volume averaged collisionalities, (b) iota at the plasma boundary, (c) normalized beta, (d) plasma inductivity, (e) toroidal beta, and (f) poloidal beta.

Internal profiles at selected times are shown in Fig. 9-5. The early NBI raises the electron temperature excluding Ohmic flux from the core. At 50 ms the central electron temperature is above a keV. The beam shine thorough peaks at 1.5 MW but decreases rapidly due to the density rise and the integral is only 80 kJ. Neither the peak nor integrated load is expected to present a problem to the device; they are well below the design capability of the beam armor tiles. The temperature profiles are not dissimilar to those expected in a device of this size. The resulting collisionalities are shown in Fig. 9-6. Both ion and electrons are collisionless in the gradient region during the high beta phase.

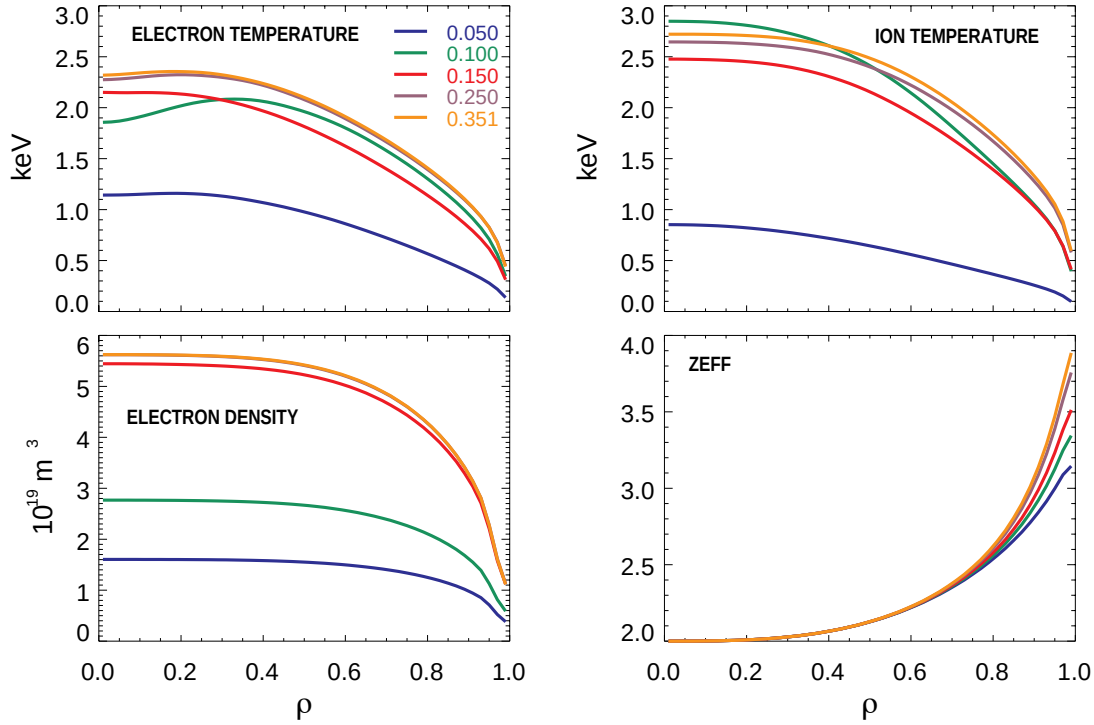

Figure 9-5. Plasma profiles. ρ is the square root of the normalized toroidal flux. The density and Z_{eff} profiles are proscribed. Temperature profiles are a result of the transport prescription.

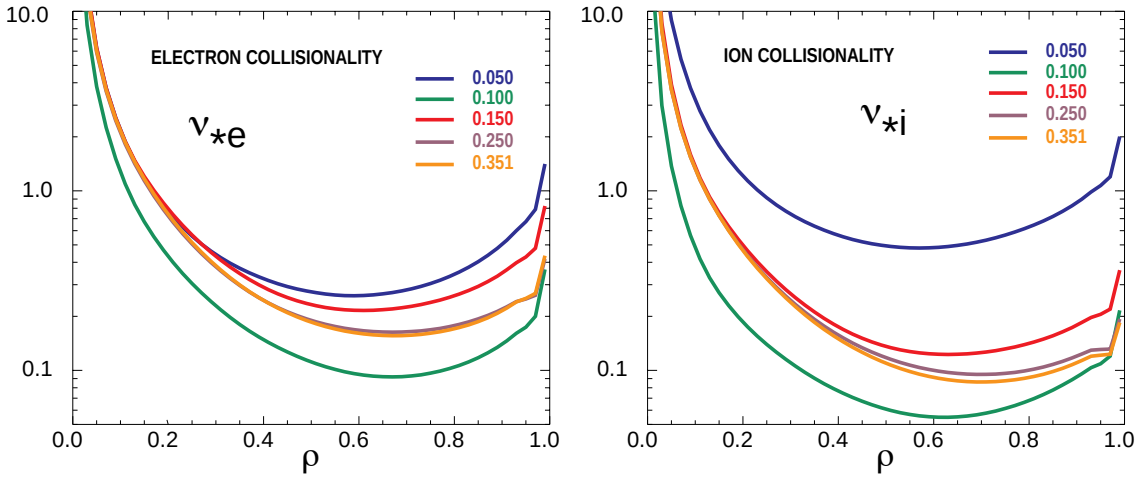

Figure 9-6. Electron and ion collisionalities at selected times. ρ is the square root of the normalized toroidal flux.

The calculation of the evolution of the current profile is the primary purpose of modeling the discharge evolution with TRANSP. The current profile comes quite close to being stationary in a 0.4 s pulse, consistent with the initial NB pulse length of 0.3 s, meeting the goal mentioned above. A true equilibration (flat voltage profile) would take quite a long time and require the planned beam upgrade. In Fig. 9-7(a) we show components of loop voltage at 303 ms. That is, we have integrated $\eta \bullet J_X$ for the individual components so we may compare them to the loop voltage. Here V_{OH} is the usual loop voltage, which will die away. V_{BS}, the bootstrap equivalent voltage vanishes at the axis, and for the computed pressure is smaller than the beam equivalent voltage, V_{NB}, for $\rho < 0.2$. Even though the net NBCD is negligible, the contribution in the core is not. While the skin time is 1 second, if one considers this small central region, the skin time is about 150 ms. When the inductive effects vanish we are left with a source term and central current density rises. Based on other scenarios we have studied, this will take an additional several hundred ms. The resulting transform profile is no longer attractive. Phase VI, the long pulse experiment, might encounter this. A solution would be alternative heating that does not produce any current, such as ICRF. In Fig. 9-7(b) the total currents are shown. At the end of the discharge the OH and NB components are balanced and the bootstrap contributes 99% of the internal current.

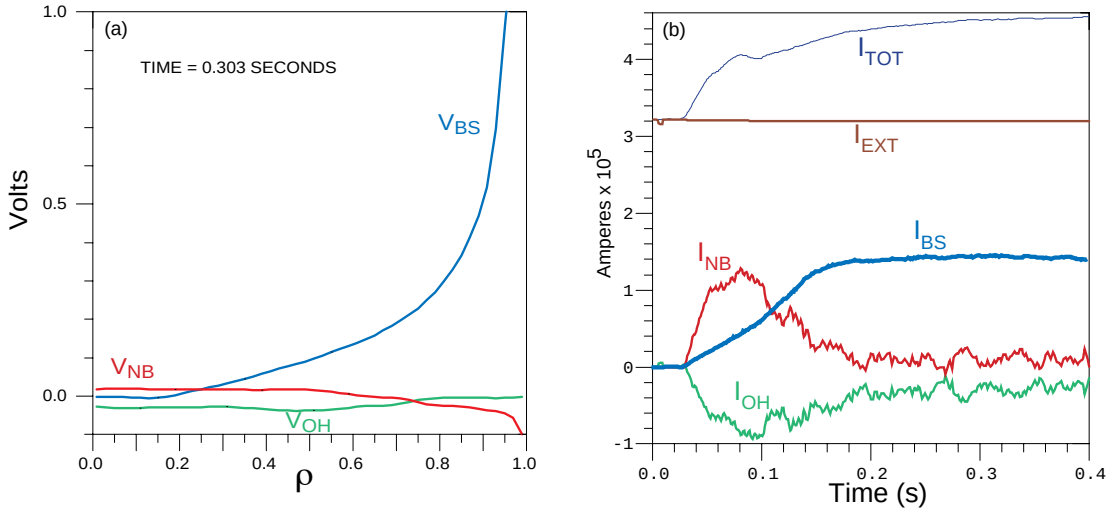

Figure 9-7. (a) The voltage profiles, for the Ohmic, bootstrap and neutral beam current sources at 303 ms. (b) Net current from all sources vs. time.

9.3 Repatriation of 2-D results to the stellarator

Having obtained a self-consistent evolution of pressure and current density, we need to follow this path in a sequence of 3D free-boundary equilibria. The input profile functions for VMEC are the pressure, p(s) and flux-surface averaged current profile, I'(s), where $s=\rho^2$. [P (ρ), and $\langle J\rangle(\rho)$ - $\langle J_{LH}\rangle(\rho)$] are extracted from the TRANSP for multiple time slices and fit to obtain the desired input functions using SVD techniques. The 3-D free-boundary equilibria are

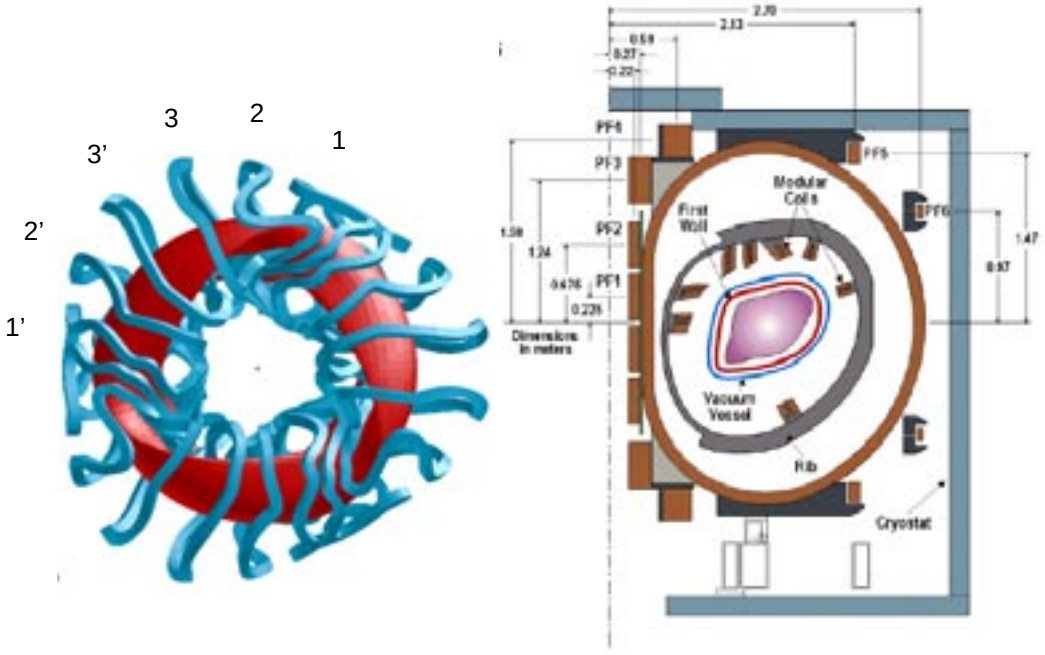

generated using STELLOPT. The coils are shown in the two pictures above. The Ohmic coils, PF1 and PF2 are not used in the optimizations presented here, but do induce the Ohmic current.

Our first task is to obtain a converged equilibrium at any time in the discharge. The coil currents need to be reasonably consistent with the plasma. Changing beta or plasma current without changing coil currents leads to poorly converged results. This is most easily done at a time corresponding to conditions near the reference equilibrium. For each time slice we optimize as described below and then use the resulting coil currents (and magnetic axis) to initialize the next time slice. This is repeated until all slices are done. We need a first slice with a well-converged equilibrium. After that calculation is largely an automated process of optimization with an initial guess from the previous case. This initial set is obtained under the constraint that the plasma boundary shape matches that of the reference case. We then proceeded through a series of optimizations to physics targets. A last step of regularizing the poloidal-field coil currents and removing interference with the vacuum vessel has not been completed at the time of this writing.

We will begin with a profile comparison between one of our cases and the PVR reference LI383 case in Fig. 9-8. We see that LI383 and the CDR reference configuration (M45h) are in close agreement while this simulation has notably different profiles. They should not be the same; the reference case has profiles scaled from the Aries-RS study while this work has different transport assumptions and the effects of Ohmic and neutral beam current drive. The lower edge iota was discussed in the last section; the pressure profile is a result of both the transport assumptions and the broad deposition of the beam energy resulting from large fast ion

orbits. One notable difference is the absence of the shearless region at ρ~0.9. A second is the edge current density. The fact that good solutions are found with these variations in the pressure and transform profiles is an indication of the robustness of this coil set. While the plasma current density dropping to negative values in the center may seem odd, recall that this current is only producing a fraction (30%) of the transform.

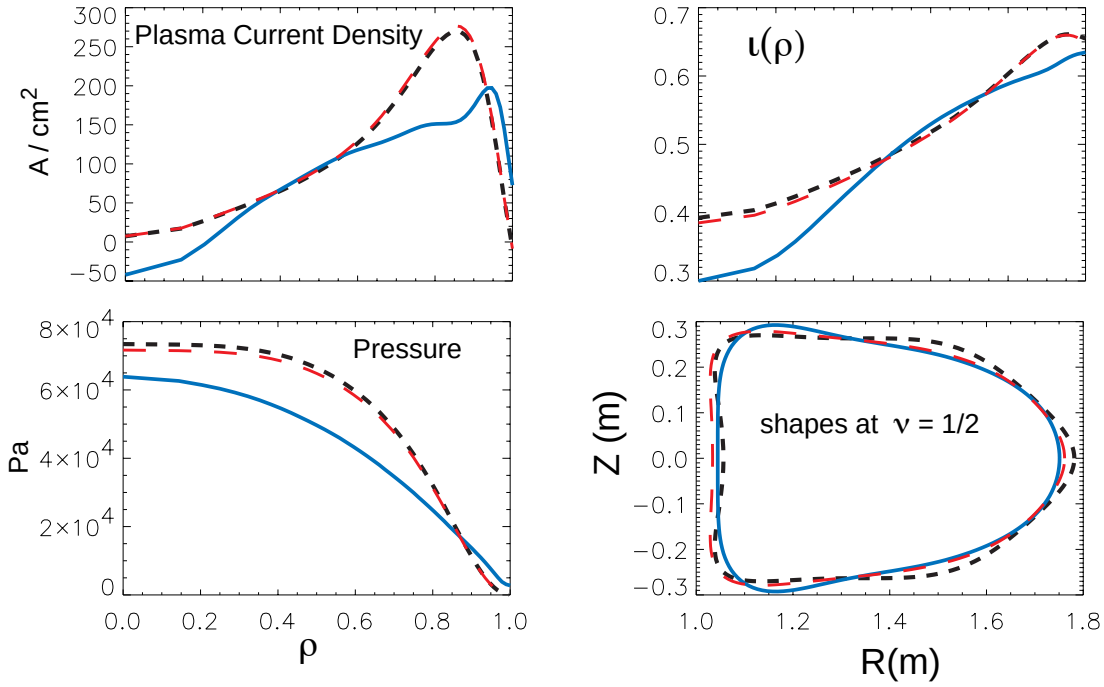

Figure 9-8. A comparison of the optimized case at 0.30 s with the LI383 fixed boundary case and the M45h reference case. Shown are plasma current density, plasma pressure and iota vs. ρ and the shapes at the half period. The black short dash is LI383, the solid blue is from these simulations and the dashed red is the M45h reference case.

For these cases we did a full optimization over aspect ratio, R·B, quasi-symmetry, the N=0 & N=1 families of ideal (no wall) kink instabilities and ballooning stability. No attempt is made to regularize the coil currents or force the plasma to fit within the vessel. Results from 30 to 400 ms are presented in Table 9-1. Recall that the simulation uses 25 ms to start, so the physical time is time-25 ms A growth rate for the kink of $< 1 \cdot 10^{-4}$ is considered negligible, that is, with minor changes in discharge programming it can be avoided. This is satisfied for all cases. The reference case is ballooning unstable in a few zones near the shearless region (43, 45,46 out of 49 zones). Ballooning is evaluated on field lines beginning both at $N_{fp}\phi = 0°$ and 60°. All the time slices in the simulated evolution are ballooning stable. Results are shown in Table 9-1. Kink growth rates are all larger than 1.e-4, which is considered negligible. The ripple diffusion ($\varepsilon^{3/2}$) is also well below a value where ripple loss would be a significant contribution to the total heat diffusivity. The results for the fixed boundary li383 case and the M45h reference case are added at the bottom of the table.

Time (ms)	Aspect Ratio	Plasma Current (A)	beta %	Distance to wall (m)	Ballooning ∑unstable	Kink (N+1) family (λ <0 stable)	Kink (N=0) Family (λ <0 stable)	Effective Ripple $\varepsilon_h^{3/2}$ (s=0.3)
30	4.368	4.57E+03	.0184	-8.31E-03	0.00E+00	1.80E-06	0	1.69E-04
40	4.379	2.95E+04	.668	-6.05E-03	0.00E+00	0	0	1.31E-04
50	4.415	5.34E+04	1.22	5.18E-03	0.00E+00	0	0	1.65E-04
70	4.405	7.78E+04	2.23	-6.25E-03	0.00E+00	8.49E-05	0	2.00E-04
80	4.391	8.56E+04	2.67	-3.63E-03	0.00E+00	0	2.10E-05	1.12E-04
100	4.39	8.16E+04	3.38	-2.68E-02	0.00E+00	3.66E-05	0	8.72E-05
110	4.443	8.86E+04	3.85	7.75E-03	0.00E+00	0	6.20E-05	1.93E-04
116	4.383	9.02E+04	3.67	-9.58E-03	0.00E+00	0	6.27E-05	9.96E-05
139	4.427	9.97E+04	3.93	2.99E-03	0.00E+00	0	0	1.33E-04
172	4.389	1.14E+05	4.06	-2.79E-03	0.00E+00	0	0	2.00E-04
203	4.452	1.20E+05	4.25	9.41E-03	0.00E+00	0	0	2.07E-04
241	4.482	1.25E+05	4.38	6.83E-03	0.00E+00	0	4.18E-05	1.52E-04
271	4.427	1.29E+05	4.53	6.50E-03	0.00E+00	0	0	1.64E-04
303	4.466	1.32E+05	4.58	1.14E-02	0.00E+00	3.09E-05	0	2.63E-04
339	4.429	1.34E+05	4.52	4.22E-03	0.00E+00	0	0	1.09E-04
378	4.436	1.33E+05	4.41	7.50E-03	0.00E+00	1.08E-05	0	1.38E-04
398	4.386	1.33E+05	4.55	-1.06E-02	0.00E+00	0	0	1.58E-04
LI383	4.365	1.75E+05	4.25	1.49E-02	1.41E-02	0	0	2.17E-05
M45h	4.366	1.75E+05	4.08	5.47E-04	4.15E-02	0	0	9.66E-05

Table 9-1. Optimization Results; Case 200202C06; R·B=2.05 m-T

Fig. 9-9 shows quantities of interest for this evolution of the stellarator plasma, NCSX. In Fig. 9-9 the transform values at the axis and plasma boundary are shown along with β, the stellarator beta which exceeds 4,5%. The distance of closet approach to the vacuum vessel, as seen in Table 9-1, needs further effort. As mentioned we have not yet optimized on this distance. The only point that appears to be a problem is at 100 ms. Noting that the nearby points are much smaller, this is just a quirk of the optimization and needs to be done again with a slightly different starting point.

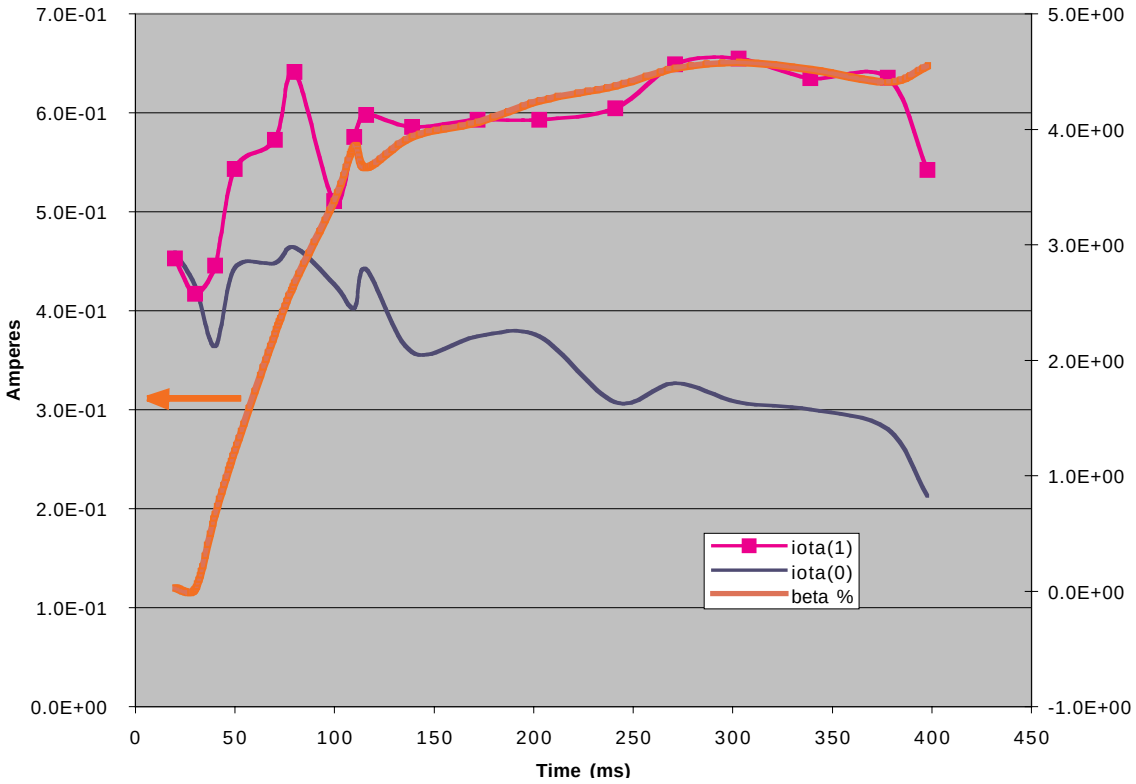

Figure 9-9. Optimization Results; Case 200202C06; R·B=2.05 m-T
Shown are ι at the axis and boundary (left scale) and β (right scale).

Table 9-2 Coil currents in amperes.

Time	MC 1	MC 2	MC 3	PF 3	PF 4	PF 5	PF 6	TF
20	-6.20E+05	-6.24E+05	-4.93E+05	-1.27E+06	2.94E+05	5.46E+05	-3.96E+05	9.85E+03
30	-5.94E+05	-5.55E+05	-4.82E+05	4.38E+06	1.16E+04	3.62E+05	-2.87E+05	-2.55E+04
40	-5.79E+05	-5.52E+05	-4.66E+05	6.57E+06	8.54E+04	-7.83E+04	7.44E+03	-3.70E+04
50	-6.36E+05	-5.83E+05	-5.13E+05	8.84E+05	7.41E+04	4.32E+05	-2.73E+05	8.04E+03
70	-6.26E+05	-6.12E+05	-4.72E+05	5.69E+06	-2.86E+04	1.55E+05	-5.70E+04	-2.08E+02
80	-6.57E+05	-6.11E+05	-5.28E+05	7.63E+05	-1.47E+04	1.69E+05	-6.63E+04	2.95E+04
100	-6.15E+05	-5.93E+05	-4.80E+05	6.45E+05	8.80E+05	2.87E+05	-1.12E+05	-8.32E+03
110	-6.62E+05	-5.44E+05	-5.36E+05	-4.33E+05	1.94E+05	1.98E+05	-6.61E+04	1.00E+04
116	-6.26E+05	-6.12E+05	-5.06E+05	4.73E+06	-3.69E+04	2.71E+05	-1.06E+05	1.21E+04
139	-6.39E+05	-5.84E+05	-5.15E+05	-1.36E+06	-3.45E+04	3.70E+05	-1.61E+05	1.00E+04
172	-6.31E+05	-5.92E+05	-4.91E+05	-4.59E+06	5.73E+05	7.03E+05	-3.81E+05	1.60E+03
203	-6.49E+05	-5.61E+05	-5.14E+05	-4.30E+06	-1.47E+04	3.38E+05	-1.44E+05	5.48E+03
241	-6.50E+05	-5.59E+05	-5.14E+05	-4.75E+06	1.48E+03	3.63E+05	-1.42E+05	5.18E+03
271	-6.69E+05	-5.48E+05	-5.18E+05	-5.63E+05	-7.32E+03	3.61E+05	-1.43E+05	8.39E+03
303	-6.92E+05	-5.34E+05	-5.34E+05	-3.76E+06	7.11E+03	3.90E+05	-1.54E+05	1.70E+04
339	-6.44E+05	-5.69E+05	-5.06E+05	-3.03E+06	3.22E+05	3.80E+05	-1.59E+05	3.33E+03
378	-6.49E+05	-5.56E+05	-5.14E+05	-3.24E+06	3.75E+03	3.75E+05	-1.55E+05	3.46E+03

398	-5.74E+05	-5.31E+05	-4.58E+05	-2.49E+06	5.32E+05	1.45E+05	-2.78E+04	-4.81E+04
Li383	0	0	0	0	0	0	0	0
M45h	-6.94E+05	-6.55E+05	-5.51E+05	1.52E+06	1.18E+06	9.52E+04	-2.31E+03	-2.78E+04

Coil currents are shown in Fig. 9-10. Notice that coil 4 is scaled by 10. This was the only coil that exhibited poor behavior. The calculations did not attempt to regularize the PF currents. In other studies (see Chapter 8) similar large PF currents were easily mapped to be within the range allowed by engineering. The final optimization of the discharge evolution scenarios is expected to remedy this also.

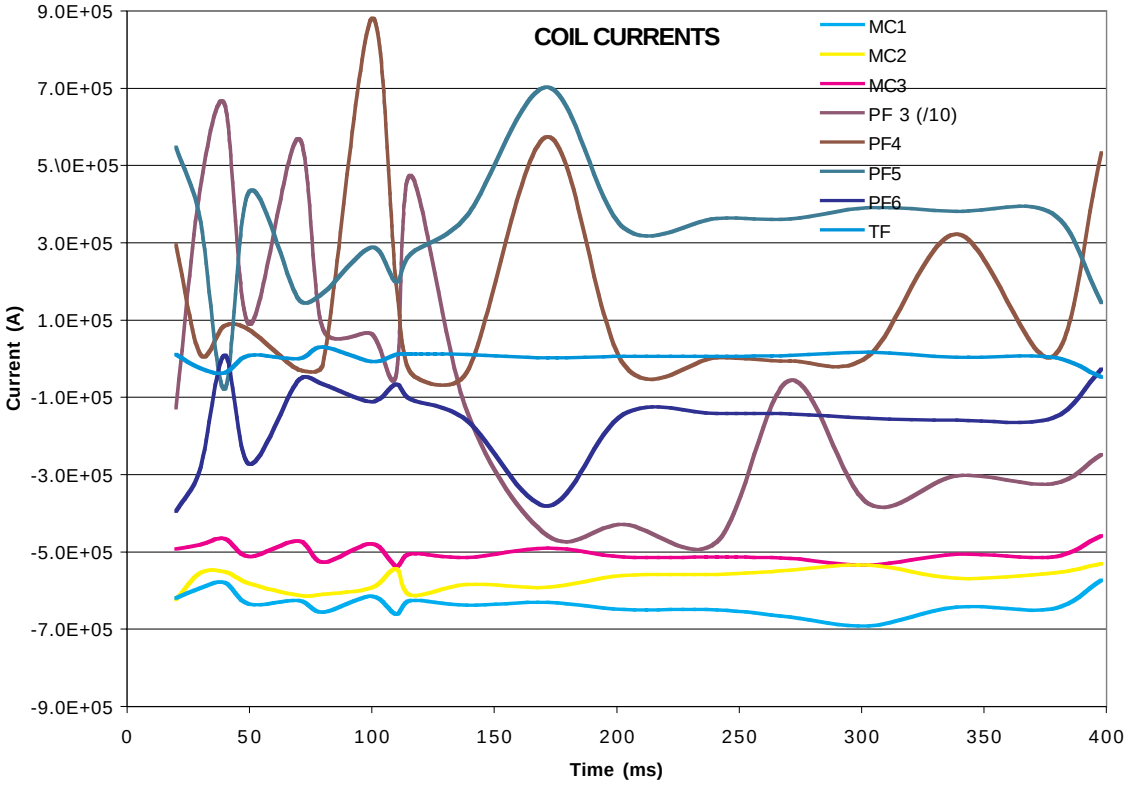

Figure 9-10. Optimization Results; Case 200202C06; R·B=2.05 m-T
Coil currents in amperes. Note that coil4 is reduced by 10.

9.4 Surface Quality

Below are a series of PIES runs for times selected from those in Table 9-1. The blue line in the figures is the original plasma boundary as calculated by VMEC, and the dashed green line indicates the location of the plasma facing components. There are several points to be made with regard to these figures. The first is that a large fraction of the plasma volume has good surfaces. This is particularly important at 303 ms where 99% of the internal current is bootstrap; there is no freedom to adjust the plasma as there is at earlier times. Second, notice the difference between 100 and 116 ms. The former does not yet have ι=0.6 in the plasma while the latter does, accounting for the island at r=0.6. Also, at 100 ms ι is near 1/2 (0.51) at the boundary and nothing untoward happens.

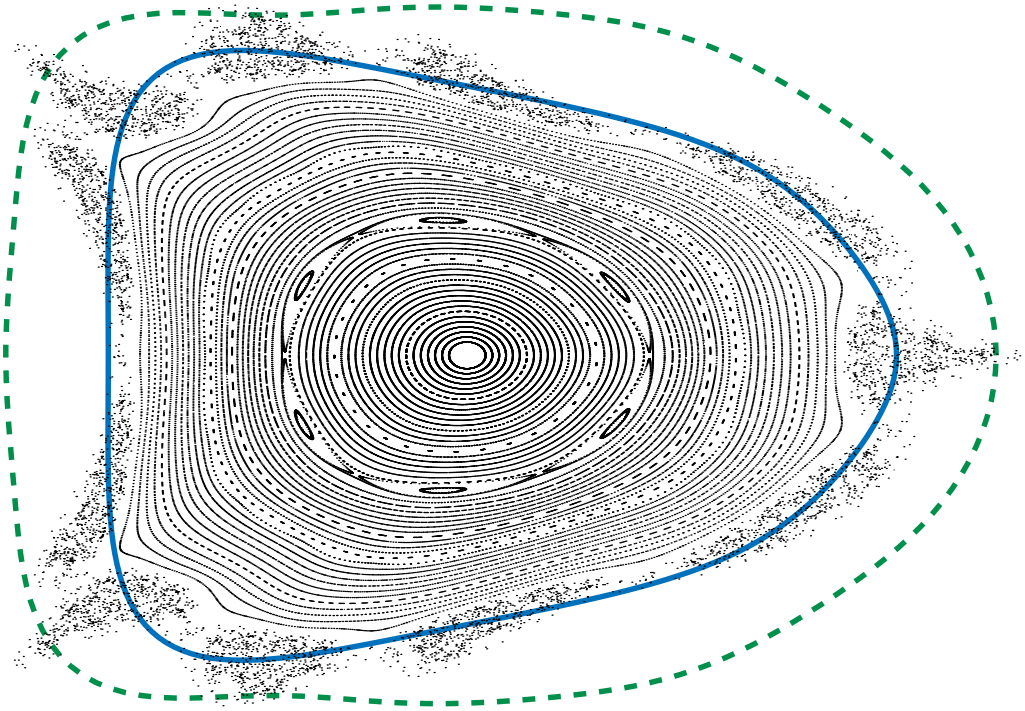

Figure 9-11. Poincare Plot. Result of PIES calculation for equilibrium at 50 ms. ι(0)=0.443, ι(1)=0.543

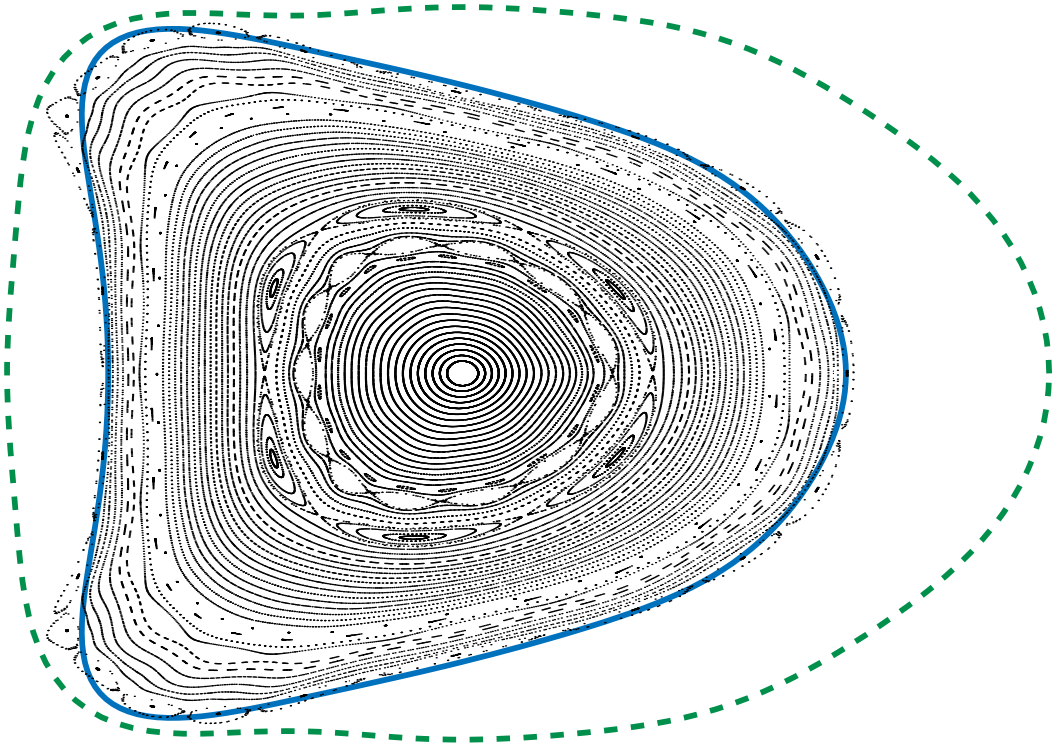

Figure 9-12. Poincare Plot. Result of PIES calculation for equilibrium at 100 ms. ι(0)=0.427, ι(1)=0.511

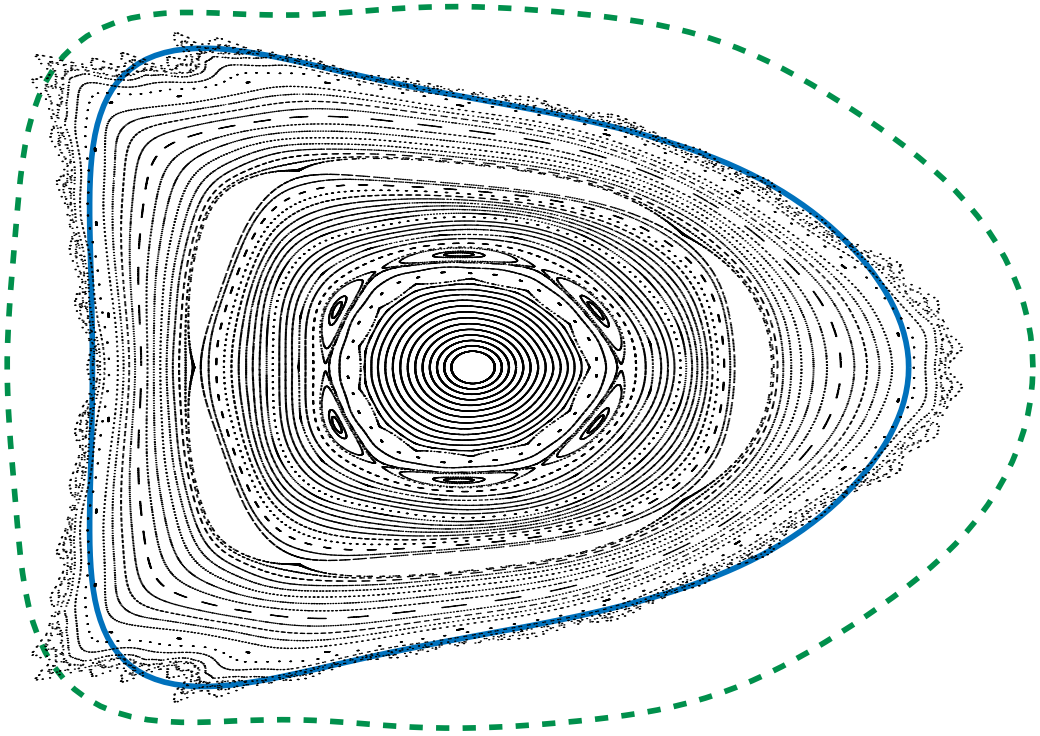

Figure 9-13. Poincare Plot. Result of PIES calculation for equilibrium at 116 ms. ι(0)=0..442, ι(1)=0.598

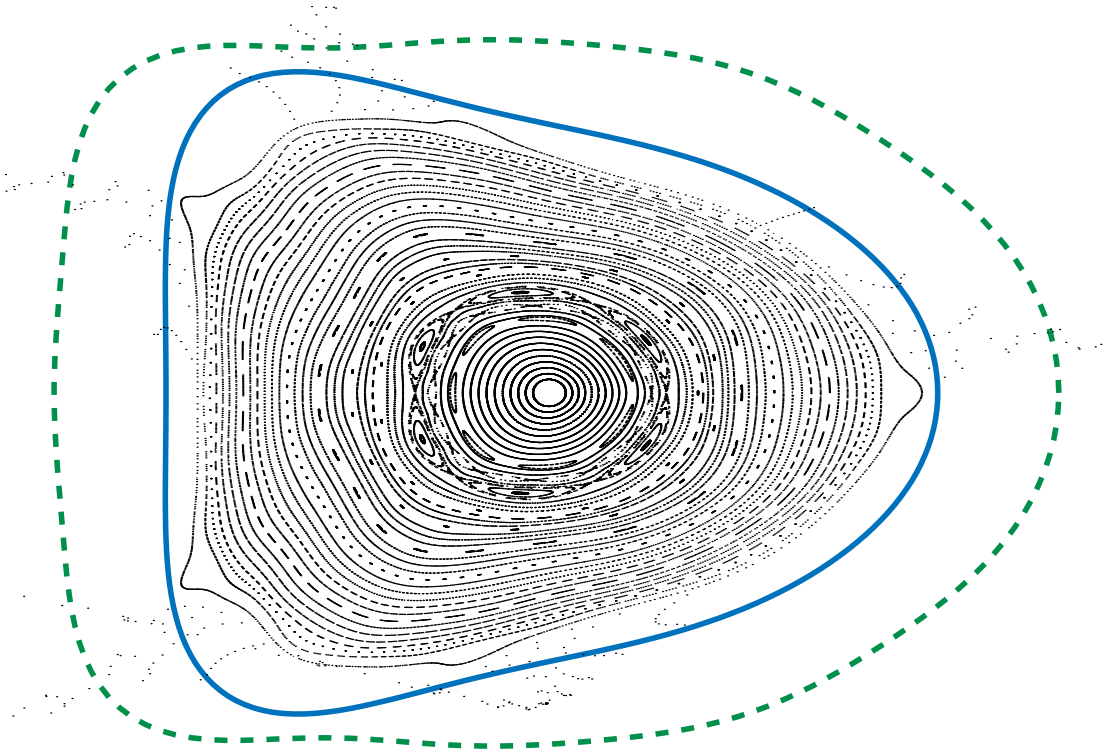

Figure 9-14. Poincare Plot. Result of PIES calculation for equilibrium at 139 ms. ι(0)=0.358, ι(1)=0.585

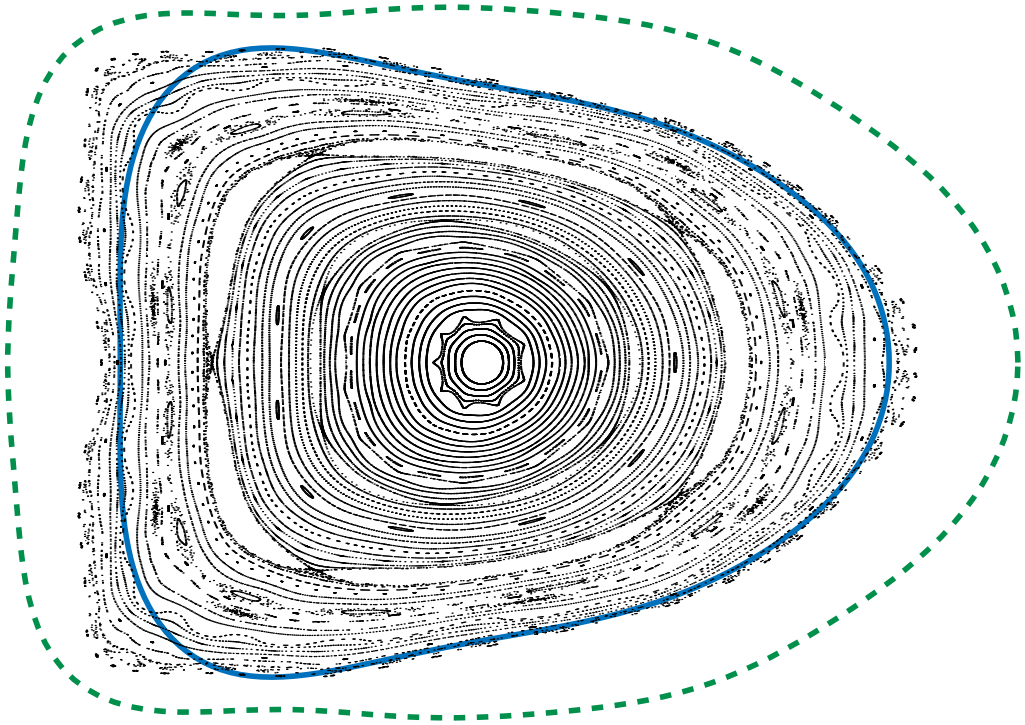

Figure 9-15. Poincare Plot. Result of PIES calculation for equilibrium at 303 ms. ι(0)=0.307, ι(1)=0.655

As discussed in Chapter 3, the PIES calculations do not include neoclassical effects, which are predicted to reduce the island widths. The m=5 island at t=303 ms, which extends over 6.3% of the cross-section, is predicted to be reduced to 3% by neoclassical effects. The m=6, 8% island at t=100 ms is predicted to be reduced to 5%. Also, PIES does not include the dynamical shielding of resonant fields by plasma rotation, as discussed in Chapter 3. This may further reduce the island widths.

These calculations have not made use of trim coils to reduce the island widths. It is expected that the trim coils will be used to reduce the widths of the m=5 and m=6 islands. Calculations of trim coil effects are in progress. Also, no attempt has been made to target surface quality in developing the startup scenario.

A number of small island chains are visible in some of the Poincare plots, particularly in the t=303 ms plot. As discussed in Chapter 3, when the island width is sufficiently small, diffusion across the island dominates diffusion along the field line, and the presence of the island has little effect on transport. This happens at a critical width of $w_0 / a \approx .08 / \sqrt{m}$, where m is the poloidal

mode number. The critical island width is about 2%-3% of the minor radius for the mode numbers of interest.

The figure below is a plot of fractional surface loss vs. time, using the data from the five PIES calculations. In calculating the flux surface loss due to islands, neoclassical effects have been included. Also, the finite ratio of diffusion across the field lines to diffusion along the field lines has been taken into account. An effective island width of $w/(1+(w_0/w)^4)$ is used, where w is the island width in the absence of this effect.

The flux surface loss at t=50 ms and t=139 ms is dominated by the loss of flux surfaces near the plasma edge, with, respectively, 6% and 11% of the cross-section lost there. At t=139 ms, the loss of flux surfaces at the plasma edge is caused by the proximity to ι=.6, with an m=5 island present just outside the plasma The trim coils may be effective in reducing this loss if the m=5 island is targeted. At t=100 ms, the flux surface loss is dominated by an m=6 island. The trim coils may be effective also in reducing this loss.

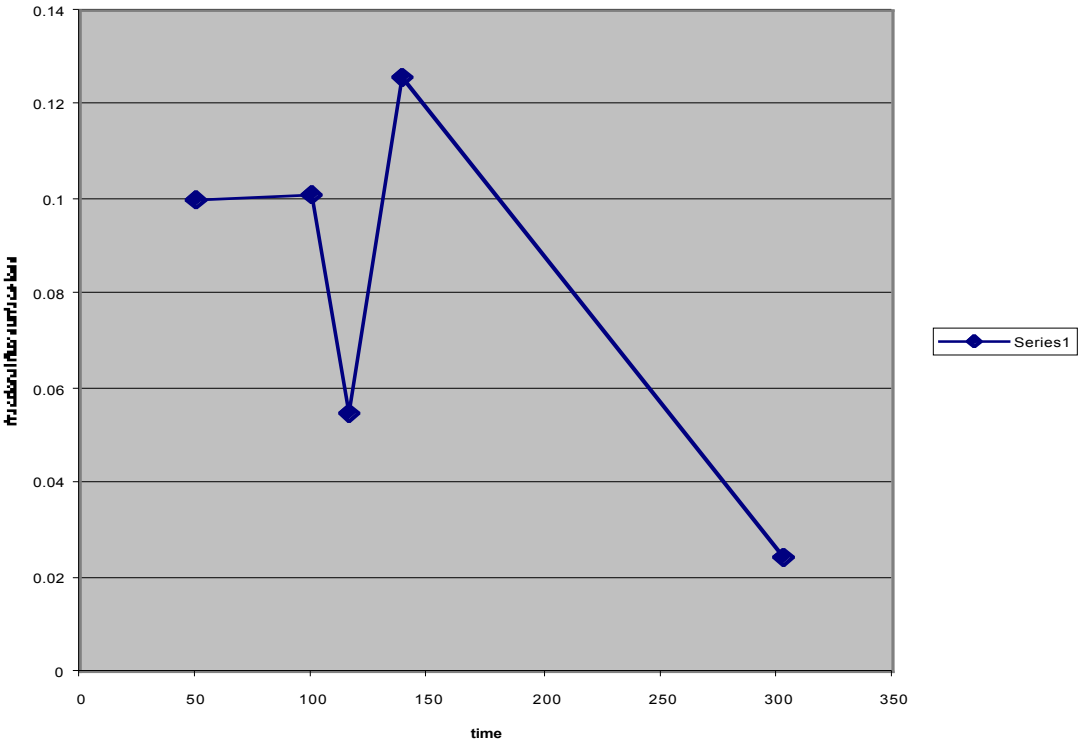

Figure 9-16. Fraction of flux surface loss to islands.

The reader will notice a characteristic change in many of the plasma shape between the PIES and VMEC boundaries; the PIES being more oblate. Shapes similar to that generated with PIES have bee observed in our studies of Ohmic plasmas, with higher l_i. PIES calculations also result in increased l_i. As PIES destroys surfaces, it renormalizes the radial coordinate and the current density, causing the current density to peak and raising iota. Assuming the physical accuracy of the model, to the calculation assumes fixed current in the external coils. However, an experiment

would run with external circuits programmed to maintain a plasma shape, and an OH transformer programmed to maintain the total current. These would change iota. Said differently, if one were able to calculate the precise discharge evolution based on VMEC equilibrium (assuming good surfaces) and then run it, one would not find the PIES states, but would not find the coil currents to be as predicted. The discharge programming is to achieve target values of fluxes and fields and these would be altered by encountering conditions where islands formed. Given the limitations of our computational models, what the actual states will be is left to experiment.

9.5 Discussion and Conclusions

Proceeding from the reference stellarator equilibrium we have constructed an "equivalent tokamak" with the vacuum transform represented as an LHCD current profile. Using this starting point in TRANSP we have evolved the plasma pressure and, along with the pressure, the self-consistent current profile to reach the target β. Such a plasma requires only L-mode confinement at B=1.4 T - but even less confinement would be adequate at lower fields. The neutral beam requirement, including the calculated losses is consistent with the planned installation of 6 MW. The simulations include fast ion effects, and we find that care must be taken to account for NBCD, particularly its effect on central iota. Tailoring the $I_P(t)$ waveform and balancing the beams to account for larger losses in the counter direction achieves a nearly stationary iota profile from the start on NBI.

Optimization over coil currents using the simulation profiles in 3-D yields a stable operating path to the target plasma while preserving good quasi-symmetry. These results are summarized in Table 9-1. Adequate stability to both kink and ballooning modes was found. This was done with the M45h coil set.